Int. J. Heat Mass Transfer. Vol. 35, No. 7, pp. 1763–1770, 1992
Printed in Great Britain

0017–9310/92 $5.00 + 0.00
© 1992 Pergamon Press Ltd

Shrinkage-induced fluid flow and domain change in two-dimensional alloy solidification

K. C. CHIANG and H. L. TSAI

Department of Mechanical and Aerospace Engineering and Engineering Mechanics, University of Missouri–Rolla, Rolla, MO 65401, U.S.A.

(*Received* 19 *October* 1990 *and in final form* 7 *June* 1991)

Abstract—The fluid flow and domain change caused by shrinkage are analyzed for the solidification of alloys in a two-dimensional rectangular cavity with riser. The system of governing equations based on the modified continuum model is solved by the SIMPLEC algorithm, and the change of domain is handled by the front tracking method. The differences between the traditional study, i.e. without considering shrinkage effect, and the present study are presented. It is found that the shrinkage-induced fluid flow and domain change enhance convective heat transfer, and the global solidification time is smaller than that predicted without the shrinkage effect.

INTRODUCTION

THE SOLID–LIQUID phase change (melting or solidification) of multiconstituent systems is important in many engineering applications, such as the making of ice, the freezing of food, the solidification of castings and ingots, crystal growth, welding, energy storage, etc. The solidification of alloys is characterized by the existence of a two-phase or mushy zone that separates the pure solid and liquid zones in the domain. Convective flow within the mushy zone is considered to be the most important and general cause of casting defects (hot tear, porosity and macrosegregation) [1–4]. Such fluid flow may be induced by shrinkage or contraction as well as by thermal and/or solutal buoyancy forces. The fluid flows driven by thermal and solutal buoyancy forces during alloy solidification have been widely investigated recently [5–7]. Literature on shrinkage-induced fluid flow during alloy solidification, however, is somewhat lacking. Flemings and Nereo [2] established a mathematical model to study macrosegregation based on the assumption that fluid flow was driven by thermal contraction only. In their model, temperature gradient and freezing rate were presumed to be known, and no attempt was made to solve the heat flow equations. Furthermore, the liquid fraction was assumed to be unaffected by the fluid flow, and the fluid flow velocity was specified without consideration of hydrodynamics. In the study of porosity, Kubo and Pehlke [3], as well as Minakawa and co-workers [4], developed mathematical models based on the assumption that the fluid flow was driven by shrinkage only. However, the energy equation used in these models was a heat conduction equation. In other words, the energy equation was uncoupled from the momentum equation, so that the advective heat flux was completely neglected.

The models proposed recently [5–7] to solve the mass, momentum, and energy equations simultaneously in the phase change systems are based on the assumption that the density of the solid phase is equal to that of the liquid phase. Hence, the fluid flow induced by shrinkage cannot be predicted by these models. Also, in these models the computational domain was assumed constant. So far, to the best knowledge of the authors, no mathematical model has been developed to handle the shrinkage-induced fluid flow and domain change during the solidification process.

The objective of the present study is to develop a mathematical model and analytical tool to simulate shrinkage-induced fluid flow during alloy solidification. The differences between the situations in which the shrinkage-induced fluid flow is omitted and considered are also investigated.

ANALYSIS

Consider a rectangular cavity with a riser located on the top filled with molten alloy, as illustrated in Fig. 1. Solidification is induced by reducing the temperature at the bottom wall to less than the solidus temperature, whereas the other walls are considered to be adiabatic.

The continuum equations developed by Bennon and Incropera [5] have been modified by Chiang [8] to include the shrinkage-induced fluid flow. In the derivation of the system of governing equations, the following simplifying assumptions are made: (1) the transport processes are laminar; (2) the properties of the solid and liquid phases are homogeneous and isotropic; (3) the solid and liquid phases in the mushy zone are in local thermal equilibrium; (4) the solid is rigid and free of internal stress; (5) the viscosity and density for each phase are constant, but can be different for the liquid and solid phases; (6) no pore for-

NOMENCLATURE

A	length of casting, Fig. 1
B, C	casting dimensions, Fig. 1
c	specific heat
C	coefficient, equation (18)
C_1	permeability coefficient, equation (17)
d	dendrite arm spacing
D	height of casting, Fig. 1
E	original height of riser, Fig. 1
f	mass fraction
g	volume fraction
h	enthalpy
k	thermal conductivity
K	permeability
L	latent heat
p	pressure
q	constant, equation (20)
t	time
T	temperature
T_l	liquidus temperature
T_s	solidus temperature
u, v	velocity components in the x and y directions
$\mathbf{V}$	velocity vector
x, y	Cartesian coordinates.

Greek symbols

β	solidification contraction
μ	dynamic viscosity
ρ	density.

Subscripts

b	condition at the bottom of the casting
i	initial condition
k	phase k
l	liquid phase
r	relative velocity between the solid and liquid phases
s	solid phase.

mation is present; (7) Newtonian phase behavior prevails; and (8) isotropic permeability exists. For the systems of interest, the conservation of equations for mass, momentum and energy can be expressed as [8]

Continuity

$$\frac{\partial}{\partial t}(\rho)+\nabla\cdot(\rho\mathbf{V})=0 \tag{1}$$

Momentum

$$\frac{\partial}{\partial t}(\rho u)+\nabla\cdot(\rho\mathbf{V}u)=\nabla\cdot\left(\mu_l\frac{\rho}{\rho_l}\nabla u\right)-\frac{\partial p}{\partial x}-\frac{\mu_l}{K}\frac{\rho}{\rho_l}(u-u_s)-\frac{C\rho^2}{K^{1/2}\rho_l}|u-u_s|(u-u_s)-\nabla\cdot(\rho f_s f_l\mathbf{V}_r u_r)+\nabla\cdot\left(\mu_l u\nabla\left(\frac{\rho}{\rho_l}\right)\right) \tag{2}$$

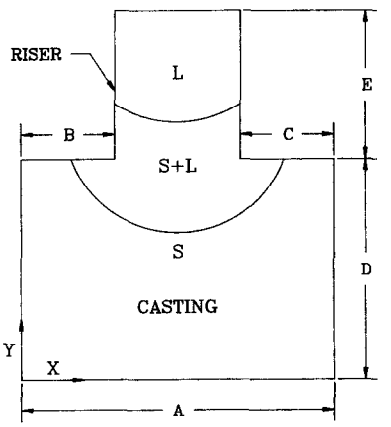

FIG. 1. Schematic of the physical domain and the coordinate system.

$$\frac{\partial}{\partial t}(\rho v)+\nabla\cdot(\rho\mathbf{V}v)=\nabla\cdot\left(\mu_l\frac{\rho}{\rho_l}\nabla v\right)-\frac{\partial p}{\partial y}-\frac{\mu_l}{K}\frac{\rho}{\rho_l}(v-v_s)-\frac{C\rho^2}{K^{1/2}\rho_l}|v-v_s|(v-v_s)-\nabla\cdot(\rho f_s f_l\mathbf{V}_r v_r)+\nabla\cdot\left(\mu_l v\nabla\left(\frac{\rho}{\rho_l}\right)\right) \tag{3}$$

Energy

$$\frac{\partial}{\partial t}(\rho h)+\nabla\cdot(\rho\mathbf{V}h)=\nabla\cdot\left(\frac{k}{c_s}\nabla h\right)+\nabla\cdot\left(\frac{k}{c_s}\nabla(h_s-h)\right)-\nabla\cdot(\rho(\mathbf{V}-\mathbf{V}_s)(h_l-h)). \tag{4}$$

The continuum density, velocity, enthalpy, and thermal conductivity are defined as

$$\rho=g_s\rho_s+g_l\rho_l \tag{5}$$

$$\mathbf{V}=f_s\mathbf{V}_s+f_l\mathbf{V}_l \tag{6}$$

$$h=f_s h_s+f_l h_l \tag{7}$$

$$k=g_s k_s+g_l k_l. \tag{8}$$

The solid mass fraction and liquid mass fraction are defined, respectively, as

$$f_s=g_s\rho_s/\rho \tag{9}$$

$$f_l=g_l\rho_l/\rho. \tag{10}$$

The phase enthalpy is defined as

$$h_k=\int_0^T c_k\,\mathrm{d}T \tag{11}$$

where c_k represents an effective specific heat of phase k. If the phase specific heats are further assumed constant, phase enthalpies by equation (11) are expressible as

$$h_s = c_s T \tag{12}$$

$$h_l = c_l T + (c_s - c_l) T_l + L \tag{13}$$

where L is the latent heat of the alloy. The continuum conservation equations are further simplified by assuming the solid phase to be stationary ($\mathbf{V}_s = 0$). This implies that the moving and settling of solid crystallite, termed the mass feeding [1], is neglected.

In general, the densities of the solid and liquid phases are not the same; therefore, some bulk motion of liquid resulting from the density difference is expected during solidification. Usually the density of the solid phase ρ_s is greater than the density of the liquid phase ρ_l (antimony, bismuth, and gallium are some exceptions). Hence, in practical foundry operations, risers are used to feed the shrinkage, and, thus, to reduce possible casting defects [1]. The riser introduces a free surface between the liquid and gas phases. The specification of boundary conditions at the free surface is quite complex. A well-known method used in the foundry to improve the efficiency of risers is to insulate them [1]. Hence, an adiabatic boundary condition at the free surface is assumed. As the shrinkage-induced fluid flow velocity is small, the free surface is considered to be flat. Hence, the effect of surface tension can be neglected. Such an assumption cannot be applied to the pure substance because of different solidification mechanisms [1].

In summary, the boundary conditions for the governing equations (1)–(4) can be written as

(1) at $x = 0$ and $0 \leqslant y \leqslant \mathrm{D}$: $u = 0, v = 0, \partial T/\partial x = 0$ (14a)

(2) at $x = \mathrm{A}$ and $0 \leqslant y \leqslant \mathrm{D}$: $u = 0, v = 0, \partial T/\partial x = 0$ (14b)

(3) at $x = \mathrm{B}$ and $\mathrm{D} \leqslant y \leqslant (\mathrm{D}+\mathrm{E})$:

$$u = 0, v = 0, \partial T/\partial x = 0 \tag{14c}$$

(4) at $x = (\mathrm{A}-\mathrm{C})$ and $\mathrm{D} \leqslant y \leqslant (\mathrm{D}+\mathrm{E})$:

$$u = 0, v = 0, \partial T/\partial x = 0 \tag{14d}$$

(5) at $y = 0$ and $0 \leqslant x \leqslant \mathrm{A}$: $u = 0, v = 0, T = T_b$ (15a)

(6) at $y = \mathrm{D}$ and $0 \leqslant x \leqslant \mathrm{B}$: $u = 0, v = 0, \partial T/\partial y = 0$ (15b)

(7) at $y = \mathrm{D}$ and $(\mathrm{A}-\mathrm{C}) \leqslant x \leqslant \mathrm{C}$:

$$u = 0, v = 0, \partial T/\partial y = 0 \tag{15c}$$

(8) at $y = (\mathrm{D}+\mathrm{E})$ and $\mathrm{B} \leqslant x \leqslant (\mathrm{A}-\mathrm{C})$:

$$p = 0, \partial u/\partial y = 0, \partial T/\partial y = 0 \tag{15d}$$

where pressure p is the gage pressure.

One should note that the last term on the right-hand side of equation (2) is identical to zero when the density difference between the solid and liquid phases is not considered. The third and fourth terms on the right-hand side of equation (2) are empirical expressions to account for the first- and second-order drag forces, respectively, between the liquid and solid phases. The fifth term on the right-hand side of equation (2) is identically zero except within the mushy region, in which f_s and f_l are not zero simultaneously. The same argument can be applied to equation (3).

The assumption of permeability in the multiphase region requires the consideration of growth morphology specific to the system under consideration. In analogy to flow in porous media, the permeability K is calculated using the Carman–Kozeny equation [9]

$$K = \frac{g_l^3}{C_l (1-g_l)^2}. \tag{16}$$

The value of C_l depends on the morphology of the porous media. In the present study C_l is expressed as [3]

$$C_l = \frac{180}{d^2} \tag{17}$$

where d, the dendritic arm spacing, is assumed to be a constant and is of the order of 10^{-2} cm. Similarly, the inertial coefficient, C, can be calculated from [10]

$$C = 0.13 g_l^{-3/2}. \tag{18}$$

In the pure solid phase ($g_l = 0$) and pure liquid phase ($g_l = 1$), equation (16) reduces to the appropriate limits, namely $K = 0$ and $K = \infty$, respectively.

Several relationships between the solid fraction g_s and the casting temperature T have been proposed in the past [1]. The rate of latent heat release is closely related to the alloy microstructure evolution during solidification, and hence is alloy dependent. In the present study, the latent heat of solidification is assumed to be released linearly between the solidus and the liquidus temperatures, and one has

$$g_s = \frac{T_l - T}{T_l - T_s} \tag{19}$$

where T_s and T_l are the solidus and liquidus temperatures of the casting, respectively.

NUMERICAL METHOD

The governing equations are in the general format suggested by Patankar [11] for the numerical solution of heat transfer and fluid flow problems; i.e. they contain a transient term, a diffusive term, a convective term, and source terms. Hence, any established numerical procedure for solving coupled elliptic partial differential equations can be used, with slight modifications for the source terms. In the present study, the equations were solved iteratively at each

time step using the control-volume-based finite difference procedure described by Patankar [11]. A fully implicit formulation was used for the time-dependent terms and the combined convection/diffusion coefficients were evaluated using an upwind scheme. The SIMPLEC algorithm [12] was applied to solve the momentum and continuity equations to obtain the velocity field. At each time-step, the momentum equation was used first in the iteration process, using the estimated volume fractions of solid and liquid for the mixture density, the permeability, and the mass fractions of solid and liquid. Then the energy equation was used to obtain the enthalpy, with which the temperature can be calculated. Next, the volume fractions of solid and liquid, the permeability, and the mass fractions of solid and liquid can be updated, and this process was repeated for each iteration step. For each time-step, iterations were terminated when the maximum residual source of mass, momentum and energy was less than 1×10^{-4}. A line-by-line solver based on the tridiagonal matrix algorithm (TDMA) was used to iteratively solve the algebraic discretization equations. The last five terms on the right-hand side of equations (2) and (3), as well as the last two terms on the right-hand side of equation (4), represent the source terms, and are treated according to the procedure outlined in ref. [11]. The fourth and fifth terms on the right-hand side of equations (2) and (3) as well as the last term on the right-hand side of equation (4) were calculated via the upwind scheme. One should note that in order to avoid the singularity in equation (2) when $g_l = 0$, equation (16) for the permeability K has been modified to

$$K = \frac{(g_l^3 + q)}{C_1 (1 - g_l)^2} \tag{20}$$

where q is a small number, say 1×10^{-24}, to suppress the fluid velocities in the solid phase.

The governing equations (1)–(4) are valid in the pure liquid and solid regions as well as in the mushy zone. Consequently, there is no need to track explicitly the geometrical shape and the extent of each region. Hence, a fixed and regular grid system can be utilized in the numerical scheme and one set of equations is solved throughout the physical domain. Special attention should be drawn to the moving boundary on the free surface at the top of the riser. As the present problem involves a distinct free surface at the top of the riser, the front tracking method [13] was employed to obtain the solutions. Moving nodes are placed at the free surface to track the physical domain of the riser. As the free surface is assumed to be flat, the movement is one-dimensional, but the momentum calculation is two-dimensional. The movement of the free surface in the riser is handled by taking the averaged velocity of the moving nodes times the time-step size.

In the calculations reported here, a grid of 31×61 points was utilized in the casting and a grid of 12×61 points was utilized in the riser. The grid was slightly skewed in the x and y directions to provide a higher concentration of nodal points near the walls of the casting and the riser, where larger velocity and thermal gradients exist. Of course, a finer grid system can provide better resolution in the numerical calculation. However, the selected mesh size here should only be viewed as a compromise between the accuracy and the computational cost. To test the accuracy of the numerical algorithm developed in this study, calculations were performed for the limiting case of cavity flow problems without phase change [8]. A good agreement was found between the predictions and the results reported in the literature.

From numerical experimentations, it was found that a larger time-step size decreased the convergence rate at the beginning of the computation. This is understandable, as the heat flux at the bottom wall is very large at the beginning of the solidification. In order to obtain optimum solution accuracy and to maintain numerical stability, a variable time-step size is adopted in the numerical calculation. The initial time-step size was 0.01 s and the maximum time-step size was 0.5 s. All the calculations were executed on Apollo 10000 workstations.

RESULTS AND DISCUSSION

Numerical calculations were performed with typical material properties for the 1% Cr–steel, from ref. [14]. These properties, casting conditions, and geometric data are summarized in Table 1. The solidification contraction, β, in Table 1 is defined as [1]

$$\beta = \frac{\rho_s - \rho_l}{\rho_s}. \tag{21}$$

The value of β for most alloys is between 2 and 8%.

Table 1. Thermophysical properties for 1% Cr steel, casting conditions and geometric data

Symbol (units)	Value
k_s (cal cm^{-1} s^{-1} K^{-1})	0.07852
k_l (cal cm^{-1} s^{-1} K^{-1})	0.06861
c_s (cal g^{-1} K^{-1})	0.15560
c_l (cal g^{-1} K^{-1})	0.15550
ρ_s (g cm^{-3})	7.36260
ρ_l (g cm^{-3})	5.89008†
$\rho_l = \rho_s$ (g cm^{-3})	6.62634‡
L (cal g^{-1})	65.9033
T_s (K)	1744.4
T_l (K)	1777.7
T_i (K)	1950.0
T_b (K)	1200.0
μ (g cm^{-1} s^{-1})	4.4122×10^{-3}
β	20%†
A (cm)	7.5
B and C (cm)	2.5
D and E (cm)	15.0

† Assumed.

‡ Density for the case without convection effect and domain change.

For the other phase change material used in the energy storage system, the value of β can be much higher. In order to see the effects of shrinkage and domain change, β is assumed to bc 20%.

The positions and shapes of the mushy region and related flow field at the selected grid points are shown in Figs. 2–4 at times $t = 75.7$, 375.7 and 1575.7 s, respectively. For clarity, the solidus and liquidus contours are also shown on the velocity plots, which represent the boundaries of the solid region, mushy region, and liquid region. From these figures, one can see that the velocity magnitude due to shrinkage is relatively small compared with that found in a typical case of forced or natural convection. The velocities are zero at the solid phase, and thereafter increase approximately with increasing y value. The maximum velocity is always at the top of the riser. The magnitude of the velocity of shrinkage-induced fluid flow is determined by the solidification rate. From Fig. 2, solidification is initially characterized by a rapid propagation of solidus and liquidus fronts, which remain nearly planar and free of irregularity. It also indicates that the solidification rate is very large at this moment. Hence, the maximum shrinkage-induced velocity in Fig. 2 is larger than that of Figs. 3 and 4.

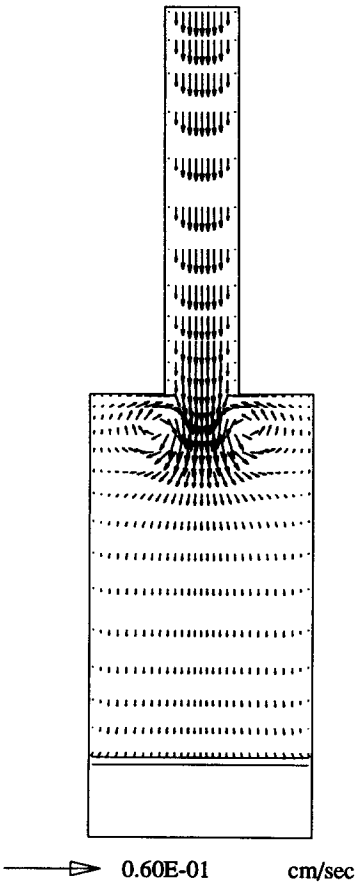

FIG. 2. The predicted flow patterns and mushy zone at time $t = 75.7$ s.

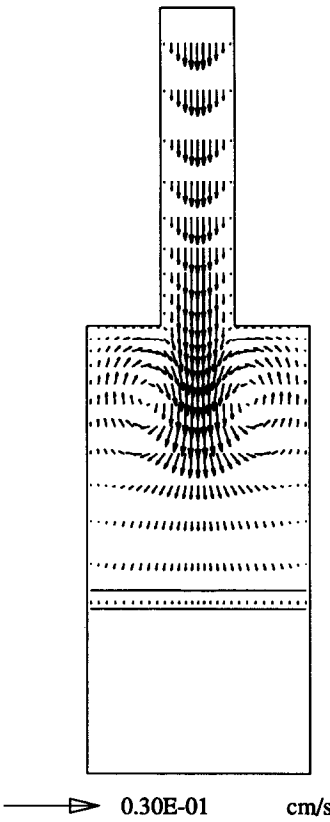

FIG. 3. The predicted flow patterns and mushy zone at time $t = 375.7$ s.

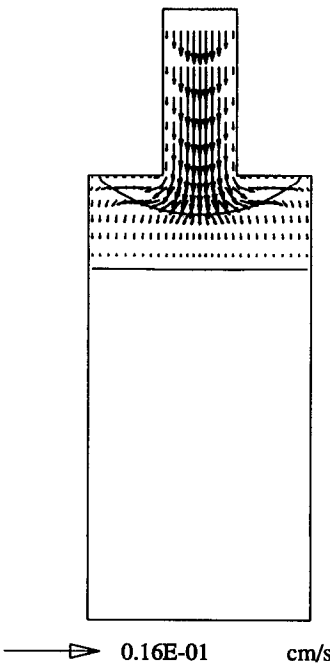

FIG. 4. The predicted flow patterns and mushy zone at time $t = 1575.7$ s.

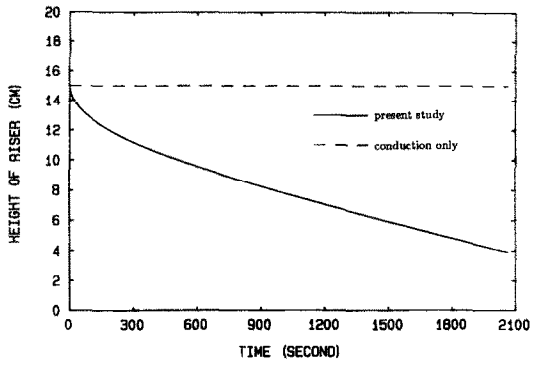

FIG. 5. The change of domain as a function of time.

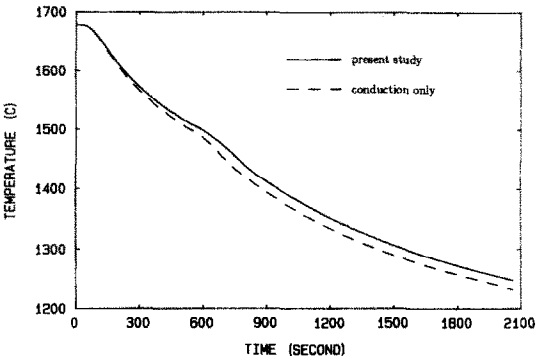

FIG. 7. A comparison of temperature history between the case of conduction only and the present study at $x = 3.75$ cm and $y = 7.50$ cm.

There are two small vortices near the intersection of the riser and the casting in Fig. 2 because of a sudden change in area. These two vortices increase in size, as shown in Fig. 3, but their strength is decreased with increasing time, due to the decrease of solidification rate. The vortices disappear gradually near the end of the solidification, as shown in Fig. 4, due to the small shrinkage-induced fluid flow and the closer proximity of the solid front to the riser, which suppresses the vortices. Due to a fine permeable matrix (dendrites) within the mushy zone, the velocities in this region are relatively smaller than those in the liquid region. Even though the velocity is small within the mushy region, such a fluid flow could be significant in determining the casting defects [1–4], especially for the case under study in which the flow is induced solely by the shrinkage.

The domain change as a function of time during solidification can be seen in Fig. 5. The horizontal dashed line in this figure represents the height of the riser, which is a constant because there is no density difference between the solid and liquid phases for the traditional study. The slope of the solid line, which denotes the result from the present study, is large at the beginning due to the large initial heat flux. The slope is decreased gradually because the solidified alloy increases the heat resistance and decreases the heat flux, which reduces the solidification rate. If the heat extraction rate is large, the shrinkage effect should be more significant. The amount of domain change is proportional to the solidification contraction, β. When the solidification contraction is large, as in the present case, the assumption of constant domain can lead to an unrealistic solution.

Comparisons of temperature history at several locations between the case without shrinkage and the present study are shown in Figs. 6–8. For the grid point near the bottom wall, the temperature histories of both cases are almost coincident, as shown in Fig. 6. The temperature for the case with shrinkage is always higher than that of the case without shrinkage (i.e. conduction only), as shown in Figs. 6 and 7. The reason for such a phenomenon is that the riser feeds hot fluid to the casting in the shrinkage-induced fluid flow case. That means the shrinkage-induced fluid flow enhances convective heat transfer. From Fig. 8, one can see that when the time is greater than about 1050 s, the temperature near the bottom of the riser for the case with shrinkage is lower than that of the case with conduction only. This phenomenon can be explained by the fact that less sensible heat is available to sustain the temperature, owing to the decrease of the height of the riser, when the shrinkage effect is taken into consideration. Therefore, the global solidification time for the casting, considering the shrink-

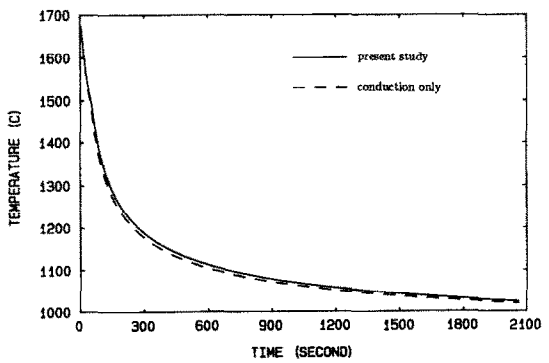

FIG. 6. A comparison of temperature history between the case of conduction only and the present study at $x = 3.75$ cm and $y = 2.17$ cm.

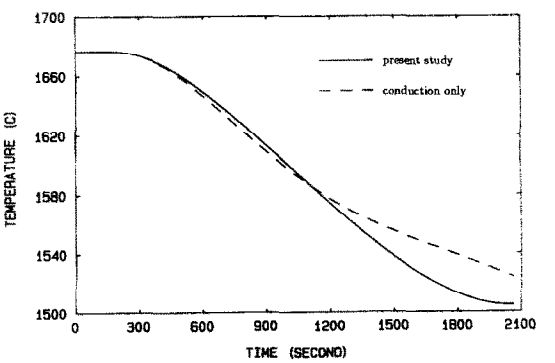

FIG. 8. A comparison of temperature history between the case of conduction only and the present study at $x = 3.75$ cm and $y = 17.62$ cm.

age effect, is less than that of the case with conduction only.

CONCLUSIONS

A mathematical model for studying the shrinkage effect during alloy solidification has been presented in this paper. The fluid flow and domain change caused solely by shrinkage were calculated for a typical alloy of 1% Cr–steel to demonstrate the significance of the shrinkage effect. From the present study, several conclusions can be summarized as follows.

(1) The shrinkage-induced fluid flow during solidification is strongly dependent on cooling conditions and solidification contraction, and its influence on the casting cooling curve could be significant.

(2) The global solidification time, which is the primary factor with which to determine the shake-out time of the casting, can be reduced by considering the shrinkage-induced fluid flow.

(3) Consideration of shrinkage-induced fluid flow could be important if one is interested in studying the flow-related casting defects, especially in the case of large density difference between the solid and liquid phases, large heat extracting rates, and weak natural convection.

Acknowledgements—This study was supported in part by the National Science Foundation under Grant No. CBT-8808212, which is gratefully acknowledged. The authors would like to thank Dr T. S. Chen for his valuable suggestions during the early stage of the present work and in the preparation of the manuscript.

REFERENCES

1. M. C. Flemings, *Solidification Processing*. McGraw-Hill, New York (1974).
2. M. C. Flemings and G. E. Nereo, Macrosegregation: part I, *Metall. Soc. AIME* **239**, 1449–1461 (1967).
3. K. Kubo and R. D. Pehlke, Mathematical modeling of porosity formation in solidification, *Metall. Trans.* **16B**, 359–365 (1985).
4. S. Minakawa, I. V. Samarasekera and F. Weiberg, Centerline porosity in plate castings, *Metall. Trans.* **16B**, 823–829 (1985).
5. W. D. Bennon and F. P. Incropera, A continuum model for momentum, heat and species transport in binary solid–liquid phase change systems—I. Model formulation, *Int. J. Heat Mass Transfer* **30**, 2161–2170 (1987).
6. V. R. Voller and C. Prakash, A fixed grid numerical modelling methodology for convection–diffusion mushy region phase-change problems, *Int J. Heat Mass Transfer* **30**, 1709–1719 (1987).
7. C. Beckermann and R. Viskanta, Double-diffusive convection during dendritic solidification of a binary mixture, *PCH PhysicoChemical Hydrodynamics* **10**, 195–213 (1988).
8. K. C. Chiang, Studies on the shrinkage-induced transport phenomena during alloy solidification, Appendix A, Ph.D. Dissertation, University of Missouri–Rolla, Rolla, MO (1990).
9. P. C. Carman, Fluid flow through granular beds, *Trans. Inst. Chem. Engr* **15**, 150–166 (1937).
10. G. S. Beavers and E. M. Sparrow, Non-Darcy flow through fibrous porous media, *J. Appl. Mech.* **36**, 711–714 (1969).
11. S. V. Patankar, *Numerical Heat Transfer and Fluid Flow*. Hemisphere, New York (1980).
12. J. P. Van Doormaal and G. D. Raithby, Enhancement of the SIMPLEC method for predicting incompressible fluid flows, *Numer. Heat Transfer* **7**, 147–163 (1984).
13. K. C. Chiang and H. L. Tsai, Transient heat transfer with change of phase in porous sand mold during casting processes, *Heat Transfer in Manufacturing and Materials Processing*, ASME HTD, Vol. 113, pp. 113–122 (1989).
14. M. K. Walther, Experimental verification of C.A.S.T., *Proc. on Modeling of Casting and Welding Processes*, pp. 345–360. The Metallurgical Society (1986).

ECOULEMENT DE FLUIDE INDUIT PAR LE RETRAIT ET CHANGEMENT DU DOMAINE DANS UNE SOLIDIFICATION BIDIMENSIONNELLE D'UN ALLIAGE

Résumé—L'écoulement du fluide et le changement de domaine causé par le retrait sont analysés pour la solidification d'alliages dans une cavité bidimensionnelle rectangulaire. Le système d'équations basées sur le modèle modifié des milieux continus est résolu par l'algorithme SIMPLEC et le changement de domaine est traité par la méthode du déplacement de front. Les différences entre l'étude traditionnelle sans considérer l'effet du retrait, et la présente étude sont présentées. On trouve que l'écoulement du fluide induit par le retrait et le changement de domaine accroissent le transfert thermique convectif, et le temps global de solidification est plus petit que ce qui est prédit sans l'effet du retrait.

FLÜSSIGKEITSBEWEGUNG UND RÄUMLICHE VERÄNDERUNG DURCH SCHRUMPFUNGSVORGÄNGE BEI DER ZWEIDIMENSIONALEN ERSTARRUNG VON LEGIERUNGEN

Zusammenfassung—Die Flüssigkeitsbewegung und die räumliche Veränderung beim Schrumpfen, verursacht durch Erstarrung einer Legierung, wird in einem zweidimensionalen rechteckigen Hohlraum mit Steiger untersucht. Das System der bestimmenden Gleichungen basiert auf einem modifizierten Kontinuumsmodell und wird mittels SIMPLEC-Algorithmus gelöst, die räumliche Veränderung mittels einer Frontfortschreitungsmethode berechnet. Die Unterschiede zu herkömmlichen Untersuchungen ohne Schrumpfung werden dargestellt. Es kann gezeigt werden, daß die Schrumpfungsvorgänge den konvektiven Wärmetransport verbessern und damit die gesamte Erstarrungszeit kleiner wird als sie ohne Schrumpfungseffekt vorhergesagt wird.

ТЕЧЕНИЕ ЖИДКОСТИ И ИЗМЕНЕНИЕ ЗАНЯТОЙ ЕЮ ОБЛАСТИ ЗА СЧЕТ УСАДКИ В ПРОЦЕССЕ ДВУМЕРНОГО ЗАТВЕРДЕВАНИЯ СПЛАВА

Аннотация—Анализируются течение жидкости и изменение области, занятой ею, при усадке в процессе затвердевания сплавов в двумерной полости прямоугольного сечения. С использованием алгоритма SIMPLEC решается система определяющих уравнений, основанная на модифицированной модели сплошной среды, и методом слежения за перемещением фронта определяется изменение области. Приведены различия между традиционным исследованием, не учитывающим эффект усадки, и представленным в данной статье. Найдено, что обусловленные усадкой течение жидкости и изменение области интенсифицируют конвективный теплоперенос и время полного затвердевания меньше рассчитанного без учета эффекта усадки.